

Role of Interlayer Electron Hopping for Spin Density Wave State in the Zero-Gap Organic Conductor

Shinya KATAYAMA*, Akito KOBAYASHI¹ and Yoshikazu SUZUMURA

Department of Physics, Nagoya University, Nagoya 464-8602

¹*Institute for Advanced Research, Nagoya University, Nagoya 464-8602*

(Received August 23, 2007)

We investigate the formation of density waves in the zero-gap state (ZGS) which has been found in the quasi-two-dimensional organic conductor α -(BEDT-TTF)₂I₃ salt under the hydrostatic pressure. The ZGS exhibits the cone-like dispersion for both the conduction band and the valence band which degenerate each other at the two-dimensional wave vectors, $\pm\mathbf{k}_0$ forming a zero gap. By using the extended Hubbard model with repulsive interaction we calculate the onset temperature of the spin density wave (SDW) as a function of the interlayer electron hopping, which by itself does not break the cone-like dispersion. It is shown that the SDW with wave number $2\mathbf{k}_0$ is induced by the combined effect of the interaction, the inter-band excitation across the zero-gap and the interlayer hopping.

KEYWORDS: α -(BEDT-TTF)₂I₃, zero-gap state, interlayer electron hopping, spin density wave, hydrostatic pressure

1. Introduction

Organic conductors, which have been investigated extensively for many years,¹ display various states due to electronic correlation, for example, superconductivity, Mott insulator or charge ordering under varying temperature or pressure.

Recently, it has been found that the 3/4-filled quasi-two-dimensional organic conductor α -(BEDT-TTF)₂I₃ salt under the uniaxial pressure along the BEDT-TTF molecule stacks (*a*-axis)² exhibits the novel electronic state described by the zero-gap state (ZGS).³ Such an exotic state appears when the Fermi surface is reduced to a point, and the valence and conduction bands degenerate at two momenta ($\pm\mathbf{k}_0$) called contact point. The linear dispersion around the contact point suggests the massless fermion. The existence of ZGS has been verified by the first principle calculation.^{4,5} The fact that the temperature dependence of the resistivity becomes weak under the high pressure^{2,6} has been analyzed by using the Born approximation⁷ where the life time of the electron is inversely proportional to the energy from the Fermi energy due to the linear density of states.

Although the ZGS is explained by the tight binding model, there are also experimental evidences² showing correlation effects in α -(BEDT-TTF)₂I₃ salt. The stripe charge ordering, which exists perpendicular to the stacking axis (*b*-axis) exists at ambient pressure and under low pressure,⁸ has been analyzed in terms of repulsive interactions by the mean field theory.⁹⁻¹¹ The origin of the superconductivity which appears with increasing the uniaxial pressure along *a*-axis, p_a , has been asserted to come from the spin fluctuation in the presence of both the charge ordering and the Fermi surface.¹² At higher pressures, the superconductivity is suppressed and the system becomes the ZGS.

The massless (or very light mass) fermion system

has been also found in graphite^{13,14} and bismuth,¹⁵ which display various properties, e. g. anomalous diamagnetism,^{13,16,17} the absence of backward scattering^{18,19} and the half-integer quantum hall effect.^{20,21} However, there are the following characteristics for the α -(BEDT-TTF)₂I₃ salt^{3,22} compared with those of graphite and bismuth. The contact point of the α -(BEDT-TTF)₂I₃ salt moves in the Brillouin zone under pressures. The Fermi velocity depends on the direction of the momentum measured from the contact point. The effective Hamiltonian²² consists of the Pauli matrices $\sigma_x, \sigma_y, \sigma_z$ and σ_0 on the bases of the wave functions for the conduction band and the valence band at \mathbf{k}_0 (or $-\mathbf{k}_0$) while that of the graphite¹³ consists of only σ_x and σ_y on the basis of site representation. The basis of these effective Hamiltonian is the Luttinger-Kohn representation²³ where wave functions are represented by the Bloch wave functions at \mathbf{k}_0 (or $-\mathbf{k}_0$). Further the interlayer electron hopping⁵ suggests new states in the ZGS of the present salt.

The ZGS state of the α -(BEDT-TTF)₂I₃ salt under the hydrostatic pressure²⁴ exhibits the anomalous behavior in the resistivity at low temperature. With decreasing temperature, there is the rise of the resistance for $T \lesssim 10$ K. The temperature dependence of the resistivity is strongly influenced by the magnetic field, which is applied to the *c*-axis being perpendicular to the conducting plane. For H above 1 T, the magnetoresistance increases again at lower temperature ($T \lesssim 10$ K) after showing a constant behavior at the intermediate region of temperature. For graphite and bismuth, the magnetoresistance has only a hump.^{26,27} Thus the increase of the resistance indicates an instability of the zero gap, which is the subject of the present paper.

As a possible state expected in the ZGS, we study the spin density wave (SDW) state under the hydrostatic pressure, which can be stabilized by the interlayer electron hopping. Applying the mean field theory to the ex-

*E-mail address: katashin@slab.phys.nagoya-u.ac.jp

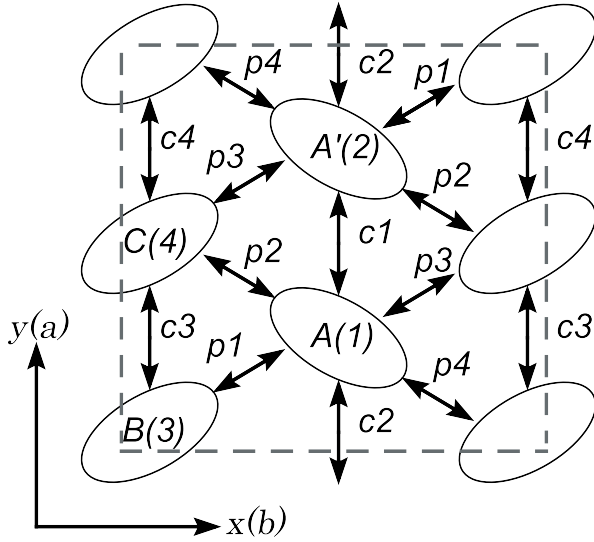


Fig. 1. Structure of the conducting plane of α -(BEDT-TTF) $_2$ I $_3$ where the unit cell is given by the dashed quadrangle, and $c1, \dots, c4, p1, \dots, p4$ denote the respective bonds corresponding to the transfer energy of the electron hopping.

tended Hubbard model, the transition temperature T_C for the SDW state is calculated where the transfer energies for the hydrostatic pressure are estimated from data of the uniaxial strain and the lattice distortion under the hydrostatic pressure. In §2, we give formulations for estimating the transfer energies under hydrostatic pressure, the charge disproportionation and the linearized gap equation for density waves. The onset temperature of the SDW state is calculated in §3. Summary and discussions are given in §4.

2. Formulation

2.1 model

The crystal structure of the α -type BEDT-TTF salt for the conducting plane is shown in Fig. 1, where a unit cell consists of four BEDT-TTF molecules (A, A', B and C). The x, y axes correspond to a, b axes in the plane, respectively, while z is the axis perpendicular to the plane. Transfer energies, which correspond to the intraplane hopping and the interplane hopping, are respectively given by

$$t_{i\alpha;j\beta} = t_A (A = c1, \dots, p4), \quad \text{and} \quad t_z \delta_{ij} \delta_{\alpha\beta}, \quad (1)$$

where i, j are the indices of the unit cell, and α and β correspond to A, A', B and C in a unit cell.

The density wave is examined by employing the extended Hubbard model,

$$\begin{aligned} H = & \sum_{n.n., \sigma} (t_{i\alpha;j\beta} a_{i\alpha\sigma}^\dagger a_{j\beta\sigma} + h.c.) \\ & + \sum_{i\alpha} U a_{i\alpha\uparrow}^\dagger a_{i\alpha\downarrow}^\dagger a_{i\alpha\downarrow} a_{i\alpha\uparrow} \\ & + \sum_{(n.n.), \sigma\sigma'} V_{i\alpha;j\beta} a_{i\alpha\sigma}^\dagger a_{j\beta\sigma'}^\dagger a_{j\beta\sigma'} a_{i\alpha\sigma}, \end{aligned} \quad (2)$$

where $a_{i\alpha\sigma}^\dagger$, ($\sigma = \uparrow, \downarrow$) denotes a creation operator of the electron and the first term is the hopping energy (eV). $n.n.$ denotes the nearest neighbor sites for both intraplane and interplane. The second and the third terms represent the on-site and nearest neighbor repulsive interactions, respectively, where $(n.n.)$ denotes the nearest neighbor site in the intraplane. The intersite interaction $V_{i\alpha;j\beta} (= V_c, V_p)$, which is considered only in a plane for the simplicity, is taken as V_c for $c1, \dots, c4$ bonds and V_p for $p1, \dots, p4$ bonds.

2.2 transfer energy under hydrostatic pressures

We estimate the intraplane transfer energy (Fig. 1) under the hydrostatic pressure by assuming the relation,

$$t_A = t_A(0)(1 + K_A^a p_a + K_A^b p_b), \quad (3)$$

where $p_a(p_b)$ is the pressure along $a(b)$ direction and $t_A(0)$ corresponds to the energy at ambient pressure. Since t_A is not known directly, coefficients K_A^a and K_A^b are estimated by using the data of the uniaxial strain. When the uniaxial strain p_a (p_b) is applied along $a(b)$ -axis, the pressure $p'_b(p'_a)$ along the $b(a)$ -axis is also added, where

$$\begin{aligned} p'_b &= r_1 p_a, \\ p'_a &= r_2 p_b. \end{aligned} \quad (4)$$

Such an additional pressure is needed to cancel out the Poisson's effect, i.e., to retain no lattice distortion along the $b(a)$ -axis. Coefficients r_1 and r_2 are estimated from the data of lattice parameters as $r_1 = 0.335$ and $r_2 = 0.257$, which are derived in Appendix.

Using eqs. (3) and (4), K_A^a and K_A^b are obtained as

$$\begin{pmatrix} K_A^a \\ K_A^b \end{pmatrix} = \frac{1}{1 - r_1 r_2} \begin{pmatrix} 1 & -r_1 \\ -r_2 & 1 \end{pmatrix} \begin{pmatrix} L_A^a \\ L_A^b \end{pmatrix}, \quad (5)$$

where

$$L_A^a \equiv \frac{1}{t_A(0)} \cdot \frac{dt_A(p_a)}{dp_a}, \quad L_A^b \equiv \frac{1}{t_A(0)} \cdot \frac{dt_A(p_b)}{dp_b}. \quad (6)$$

Quantities L_A^a and L_A^b denote the variation of transfer energies with respect to uniaxial strain p_a and p_b , respectively. Equation (6) is calculated from the transfer energies under the ambient pressure, a -axis strain at 2 kbar and b -axis strain at 3 kbar^{3, 28} (see Table I). Substituting r_1, r_2, L_A^a and L_A^b into eq. (5), we obtain the transfer energy, $t_A(p) = t_A(0)(1 + (K_A^a + K_A^b)p)$ for the hydrostatic pressure, where $K_A^a + K_A^b$ are given in Table I.

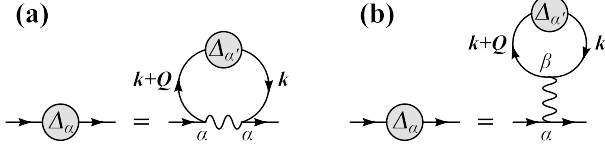
2.3 charge disproportionation

Next, we calculate the density $\langle n_\alpha \rangle (= (1/N) \sum_{i\sigma} \langle a_{i\alpha\sigma}^\dagger a_{i\alpha\sigma} \rangle)$ by using the self-consistent Hartree approximation, which gives the nonmagnetic state and the ZGS. The charge disproportionation corresponds to the spatial variation of $\langle n_\alpha \rangle$. In a way similar to previous studies,^{10-12, 22} the self-consistent equations for the density at the respective site α are written as ($\mathbf{k} = (k_x, k_y, k_z)$)

$$\langle n_\alpha \rangle = 2 \sum_{\gamma=1}^4 |d_{\alpha\gamma}(\mathbf{k})|^2 \frac{1}{\exp[\xi_\gamma(\mathbf{k})/T] + 1}, \quad (7)$$

Table I. Transfer energy per unit pressure, which is normalized by $t_A(0)$. L_A^a and L_A^b are obtained in Ref. 3 based on Ref. 28.

A	$c1$	$c2$	$c3$	$c4$	$p1$	$p2$	$p3$	$p4$
a -axis strain (L_A^a)	0.167	-0.025	0.089	0.089	0.011	0.0	0.0	0.032
b -axis strain (L_A^b)	0.042	0.133	0.167	0.167	0.024	0.022	0.053	0.032
Hydrostatic pressure ($K_A^a + K_A^b$)	0.166	0.077	0.194	0.194	0.026	0.016	0.039	0.042

Fig. 2. Feynman diagrams for $\Delta_{Q\alpha}^{Sx}$ and $\Delta_{Q\alpha}^{Sy}$ in eq. (18) (a), and that for $\Delta_{Q\alpha}^{Sz}$ in eq. (18) and $\Delta_{Q\alpha}^C$ in eq. (19) (b).

where

$$\sum_{\beta=1}^4 (\varepsilon_{\alpha\beta}(\mathbf{k}) + t_\alpha \delta_{\alpha\beta} - \mu \delta_{\alpha\beta}) d_{\beta\gamma}(\mathbf{k}) = \xi_\gamma(\mathbf{k}) d_{\alpha\gamma}(\mathbf{k}), \quad (8)$$

$$\varepsilon_{\alpha\beta}(\mathbf{k}) = \frac{1}{N} \sum_{(n.n.)} t_{i\alpha;j\beta} e^{-i\mathbf{k}(\mathbf{r}_i - \mathbf{r}_j)} + 2t_z \cos k_z \delta_{\alpha\beta}, \quad (9)$$

$$t_\alpha = \frac{U \langle n_\alpha \rangle}{2} + \frac{1}{N} \sum_{(n.n.)} V_{i\alpha;j\beta'} \langle n_{\beta'} \rangle. \quad (10)$$

N is the number of the unit cell. For eqs. (7) and (8), we used the Fourier transformation expressed as $a_{i\alpha\sigma} = (1/\sqrt{N}) \sum_{\mathbf{k}} c_{\mathbf{k}\alpha\sigma} e^{-i\mathbf{k} \cdot \mathbf{r}_i}$. We take the lattice constant as unity. The band index γ is taken as the descending order of $\xi_\gamma(\mathbf{k})$, i.e., $\xi_1(\mathbf{k}) > \xi_2(\mathbf{k}) > \xi_3(\mathbf{k}) > \xi_4(\mathbf{k})$. The quantity μ is the chemical potential determined by a condition, $\sum_\alpha \langle n_\alpha \rangle = 6$, due to 3/4 filling. The effect of t_z on the charge disproportionation and μ is negligibly small, e.g., $\langle \delta n_\alpha \rangle \sim 10^{-5}$ and $\delta\mu \sim 10^{-5}$ eV in the present calculation of $t_z \sim 0.003$. The temperature (T) is taken as $T \rightarrow 0$ in calculating the charge disproportionation, since the T dependence of $\langle n_\alpha \rangle$ is negligibly small at temperatures for the onset of SDW. The parameters of U, V_p, V_c and p are chosen to obtain the ZGS state in the presence of charge disproportionation.

2.4 transition temperature for density waves

Now, we calculate the transition temperature, T_C , corresponding to the onset temperature for the density waves, where the operator of the spin density waves, ($S_{Q\alpha}^x(\mathbf{k}), S_{Q\alpha}^y(\mathbf{k}), S_{Q\alpha}^z(\mathbf{k})$) and that of the charge density wave ($C_{Q\alpha}(\mathbf{k})$), are defined, respectively, as ($\mathbf{Q} = (q_x, q_y, q_z)$)

$$\begin{aligned} S_{Q\alpha}^x(\mathbf{k}) &= (c_{\mathbf{k}+\mathbf{Q}\alpha\uparrow}^\dagger c_{\mathbf{k}\alpha\downarrow} + c_{\mathbf{k}+\mathbf{Q}\alpha\downarrow}^\dagger c_{\mathbf{k}\alpha\uparrow})/2, \\ S_{Q\alpha}^y(\mathbf{k}) &= -i(c_{\mathbf{k}+\mathbf{Q}\alpha\uparrow}^\dagger c_{\mathbf{k}\alpha\downarrow} - c_{\mathbf{k}+\mathbf{Q}\alpha\downarrow}^\dagger c_{\mathbf{k}\alpha\uparrow})/2, \\ S_{Q\alpha}^z(\mathbf{k}) &= (c_{\mathbf{k}+\mathbf{Q}\alpha\uparrow}^\dagger c_{\mathbf{k}\alpha\uparrow} - c_{\mathbf{k}+\mathbf{Q}\alpha\downarrow}^\dagger c_{\mathbf{k}\alpha\downarrow})/2, \\ C_{Q\alpha}(\mathbf{k}) &= (c_{\mathbf{k}+\mathbf{Q}\alpha\uparrow}^\dagger c_{\mathbf{k}\alpha\uparrow} + c_{\mathbf{k}+\mathbf{Q}\alpha\downarrow}^\dagger c_{\mathbf{k}\alpha\downarrow})/2. \end{aligned} \quad (11)$$

In terms of eq. (11), the second and third terms of eq. (2) can be rewritten as

$$\begin{aligned} & \sum_{i\alpha} U a_{i\alpha\uparrow}^\dagger a_{i\alpha\downarrow}^\dagger a_{i\alpha\downarrow} a_{i\alpha\uparrow} \\ &= -\frac{1}{N} \sum_{\mathbf{k}\mathbf{k}'\mathbf{Q}\alpha} U (S_{-\mathbf{Q}\alpha}^x(\mathbf{k}') S_{\mathbf{Q}\alpha}^x(\mathbf{k}) + S_{-\mathbf{Q}\alpha}^y(\mathbf{k}') S_{\mathbf{Q}\alpha}^y(\mathbf{k})) \\ &= \frac{1}{N} \sum_{\mathbf{k}\mathbf{k}'\mathbf{Q}\alpha} U (C_{-\mathbf{Q}\alpha}(\mathbf{k}') C_{\mathbf{Q}\alpha}(\mathbf{k}) - S_{-\mathbf{Q}\alpha}^z(\mathbf{k}') S_{\mathbf{Q}\alpha}^z(\mathbf{k})) \end{aligned} \quad (12)$$

and

$$\begin{aligned} & \sum_{(n.n.),\sigma\sigma'} V_{i\alpha;j\beta} a_{i\alpha\sigma}^\dagger a_{j\beta\sigma'}^\dagger a_{j\beta\sigma'} a_{i\alpha\sigma} \\ &= \frac{1}{N} \sum_{\mathbf{k}\mathbf{k}'\mathbf{Q}\alpha\beta} 2V_{\alpha\beta}(\mathbf{Q}) C_{-\mathbf{Q}\beta}(\mathbf{k}') C_{\mathbf{Q}\alpha}(\mathbf{k}), \end{aligned} \quad (13)$$

respectively. The matrix elements of $V_{\alpha\beta}(\mathbf{Q})$ are given as

$$\begin{aligned} V_{\alpha\alpha}(\mathbf{Q}) &= 0, \\ V_{12}(\mathbf{Q}) &= V_c(1 + e^{-iq_y}), \\ V_{13}(\mathbf{Q}) &= V_p(1 + e^{iq_x}), \\ V_{14}(\mathbf{Q}) &= V_p(1 + e^{iq_x}), \\ V_{23}(\mathbf{Q}) &= V_p(e^{iq_x} + e^{i(q_x+q_y)}), \\ V_{24}(\mathbf{Q}) &= V_p(1 + e^{iq_x}), \\ V_{34}(\mathbf{Q}) &= V_c(1 + e^{-iq_y}), \end{aligned} \quad (14)$$

and $V_{\alpha\beta}(\mathbf{Q}) = V_{\beta\alpha}^*(\mathbf{Q})$. Applying the mean field approximation, eq. (2) is expressed as

$$\begin{aligned} H_{\text{MF}} &= \sum_{\mathbf{k}\gamma\sigma} \xi_\gamma(\mathbf{k}) c_{\mathbf{k}\gamma\sigma}^\dagger c_{\mathbf{k}\gamma\sigma} \\ &+ \sum_{\mathbf{k}\mathbf{Q}\alpha} \left[\Delta_{Q\alpha}^{Sx} S_{Q\alpha}^x(\mathbf{k}) + \Delta_{Q\alpha}^{Sy} S_{Q\alpha}^y(\mathbf{k}) + h.c. \right] \end{aligned} \quad (15)$$

or

$$\begin{aligned} H_{\text{MF}} &= \sum_{\mathbf{k}\gamma\sigma} \xi_\gamma(\mathbf{k}) c_{\mathbf{k}\gamma\sigma}^\dagger c_{\mathbf{k}\gamma\sigma} \\ &+ \sum_{\mathbf{k}\mathbf{Q}\alpha} \left[\Delta_{Q\alpha}^{Sz} S_{Q\alpha}^z(\mathbf{k}) + \Delta_{Q\alpha}^C C_{Q\alpha}(\mathbf{k}) + h.c. \right], \end{aligned} \quad (16)$$

where $\Delta_{Q\alpha}^\zeta$ ($\zeta = x, y, z$) and $\Delta_{Q\alpha}^C$ are the order parameters of the SDW and CDW state defined as

$$\begin{aligned} \Delta_{Q\alpha}^{S\zeta} &= -\frac{1}{N} \sum_{\mathbf{k}} U \langle S_{-\mathbf{Q}\alpha}^\zeta(\mathbf{k}) \rangle \\ \Delta_{Q\alpha}^C &= \frac{1}{N} \sum_{\mathbf{k}\beta} (U \delta_{\alpha\beta} + 2V_{\alpha\beta}(\mathbf{Q})) \langle C_{-\mathbf{Q}\beta}(\mathbf{k}) \rangle. \end{aligned} \quad (17)$$

The quantity $\xi_\gamma(\mathbf{k})$ in eqs. (15) and (16) is the kinetic energy, which exhibits the cone-like dispersion and the zero gap located between $\xi_1(\mathbf{k})$ and $\xi_2(\mathbf{k})$. The quantity $c_{\mathbf{k}\gamma\sigma} (= \sum_\alpha d_{\alpha\gamma}^*(\mathbf{k})c_{\mathbf{k}\alpha\sigma})$ is the annihilation operator for the particle with the wave number \mathbf{k} and spin σ in the band γ .

The transition temperature T_C for the density wave is calculated by using the linearized gap equations for $\Delta_{\mathbf{Q}\alpha}^{S\zeta}$, ($\zeta = x, y, z$) and $\Delta_{\mathbf{Q}\alpha}^C$, which are shown in Fig. 2. They are written explicitly as

$$\lambda^S \Delta_{\mathbf{Q}\alpha}^{S\zeta} = \sum_{\alpha'\gamma\gamma'} U I_{\gamma\gamma'}(\mathbf{Q}; \alpha, \alpha') \Delta_{\mathbf{Q}\alpha'}^{S\zeta} \quad (18)$$

$$\begin{aligned} \lambda^C \Delta_{\mathbf{Q}\alpha}^C = & - \sum_{\beta\alpha'\gamma\gamma'} (U\delta_{\alpha\beta} + 2V_{\alpha\beta}(\mathbf{Q})) \\ & \times I_{\gamma\gamma'}(\mathbf{Q}; \beta, \alpha') \Delta_{\mathbf{Q}\alpha'}^C, \end{aligned} \quad (19)$$

where $I_{\gamma\gamma'}(\mathbf{Q}; \alpha, \beta)$ is defined as

$$\begin{aligned} I_{\gamma\gamma'}(\mathbf{Q}; \alpha, \beta) = & -\frac{1}{N} \sum_{\mathbf{k}} \frac{f(\xi_\gamma(\mathbf{k} + \mathbf{Q})) - f(\xi_{\gamma'}(\mathbf{k}))}{\xi_\gamma(\mathbf{k} + \mathbf{Q}) - \xi_{\gamma'}(\mathbf{k})} \\ & \times d_{\alpha\gamma}(\mathbf{k} + \mathbf{Q}) d_{\alpha\gamma'}^*(\mathbf{k}) d_{\beta\gamma}^*(\mathbf{k} + \mathbf{Q}) d_{\beta\gamma'}(\mathbf{k}) \end{aligned} \quad (20)$$

and $f(x) (= [e^{x/T} + 1]^{-1})$ is the Fermi distribution function. The transition temperature of the density wave is obtained from the condition $\lambda^S = 1$ or $\lambda^C = 1$. We note that spin response parallel to the quantized axis (z -axis) is the same as that of perpendicular to the z -axis due to isotropic properties for both interactions and transfer energies. The summation of γ and γ' in eqs. (18) and (19) takes only the conduction band ($\gamma = 1$) and the valence band ($\gamma = 2$) since the density wave in the present calculation is determined essentially by these two bands. Hereafter, the units of the pressure and energy are taken as kbar and eV, respectively. We also use the two-dimensional component of \mathbf{Q} , i.e.,

$$\mathbf{Q} \equiv \mathbf{q} + q_z \mathbf{e}_z, \quad (21)$$

where $\mathbf{q} = (q_x, q_y)$ and \mathbf{e}_z is the unit vector perpendicular to the conducting plane.

3. Spin Density Wave

Before studying the SDW state, we describe the state where the interlayer transfer is absent. The ZGS under the hydrostatic pressure is found as follows. When only the kinetic energy is taken into account, i.e., without the Coulomb interaction, the Fermi surface exists for $0 < p < 5.4$ where the contact point is located below the Fermi energy. With increasing the pressure, the Fermi surface becomes small and the ZGS is obtained for $p > 5.4$. The introduction of interactions suppresses the ZGS state. When we take a set of parameters, $U = 0.4, V_p = 0.05, V_c = 0.17^{12}$ as is used in the present calculation, there exists the insulating state with the stripe charge order for $0 < p < 2.1$, the metallic state with the charge order for $2.1 < p < 12.5$, and finally the ZGS for $p > 12.5$.

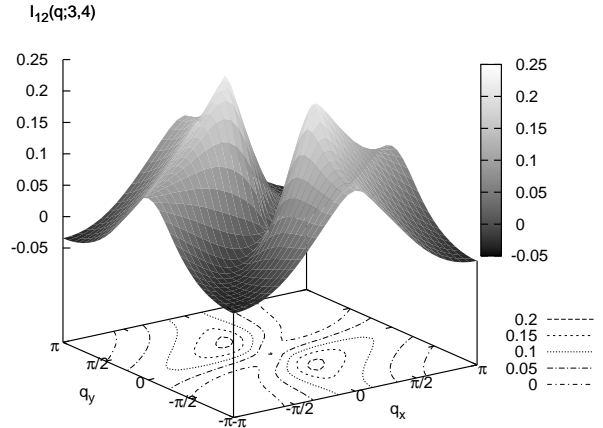


Fig. 3. \mathbf{q} -dependence of $I_{12}(\mathbf{q}; \alpha, \beta)$ ($(\alpha, \beta) = (3, 4)$) for $U = 0.4, V_c = 0.17, V_p = 0.05$ and $p = 16$, where the contact points exist on $\mathbf{k}_0 = (\pm 0.970\pi, \pm 0.216\pi)$. The temperature is chosen as $T = 0.001$.

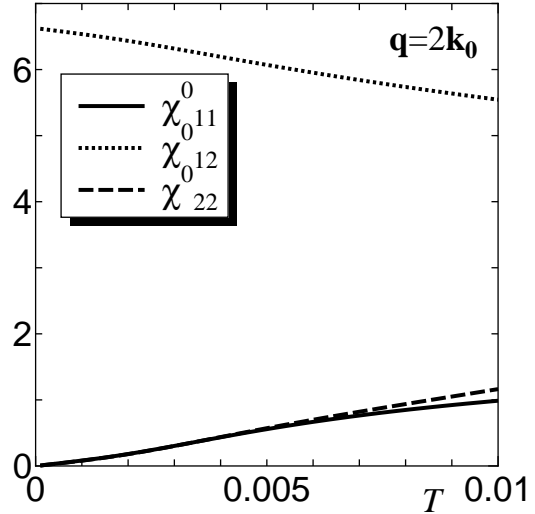


Fig. 4. T -dependence of the bare susceptibility, $\chi_{\gamma\gamma'}^0(\mathbf{q})$ for $U = 0.4, V_c = 0.17, V_p = 0.05$ and $p = 16$. The cases for $(\gamma, \gamma') = (1, 1), (2, 2)$ and $(1, 2)$ are plotted by solid, dashed and dotted line, respectively. The $(2, 1)$ component of the susceptibility is equal to the $(1, 2)$ component. The wave number is taken as $\mathbf{q} = 2\mathbf{k}_0 = (-0.060\pi, 0.432\pi)$.

3.1 density waves in the absence of t_z

We examine the property of $I_{\gamma\gamma'}(\mathbf{q}; \alpha, \beta)$ for $t_z = 0$. The density response function of eq. (20) consists of the intra-band components I_{11} and I_{22} and the inter-band component $I_{12} (= I_{21})$ where the main contribution comes from the inter-band one having the effect similar to the nesting condition. Figure 3 shows the \mathbf{q} dependence of $I_{\gamma\gamma'}(\mathbf{q})$ with $\mathbf{q} = (q_x, q_y)$ (no q_z dependence due to $t_z = 0$). Since there are maxima at $\mathbf{q} = \pm 2\mathbf{k}_0 = (\mp 0.060\pi, \pm 0.432\pi)$, the incommensurate density wave with $\mathbf{q} = \pm 2\mathbf{k}_0$ is expected from $I_{12}(\mathbf{q})$ and $I_{21}(\mathbf{q})$, i.e., the main contribution is given by an excitation from the valence band ($\gamma = 2$) to the conduction band ($\gamma = 1$) close to ε_F around \mathbf{k}_0 .

For the clear understanding of the effect of tempera-

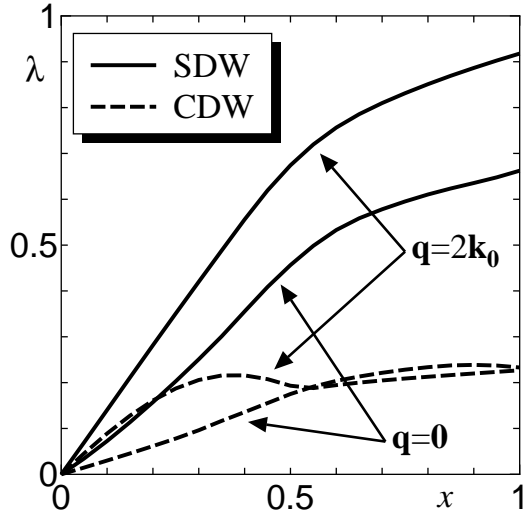


Fig. 5. x -dependence of λ for the SDW (solid line) and CDW (dashed line) with $\mathbf{q} = 0, 2\mathbf{k}_0$, where $p = 16$ and $T = 0.001$. The strength of the Coulomb interaction x is defined as $U = 0.4x$, $V_c = 0.17x$, $V_p = 0.05x$.

ture on the $2\mathbf{k}_0$ density response, we calculate the susceptibility defined as

$$\chi_{\gamma\gamma'}^0(\mathbf{q}) = -\frac{1}{N} \sum_{\mathbf{k}} \frac{f(\xi_{\gamma}(\mathbf{k} + \mathbf{q})) - f(\xi_{\gamma'}(\mathbf{k}))}{\xi_{\gamma}(\mathbf{k} + \mathbf{q}) - \xi_{\gamma'}(\mathbf{k})}. \quad (22)$$

The temperature dependence of $\chi_{\gamma\gamma'}^0(2\mathbf{k}_0)$ is shown in Fig. 4. With decreasing temperature, the diagonal component, $\chi_{\gamma\gamma}^0(2\mathbf{k}_0)$, corresponding to the intra-band process, decreases and reduces to zero in the limit of zero temperature due to the vanishing of the density of states at the Fermi energy. However, the off-diagonal component of $\chi_{12}^0(2\mathbf{k}_0)$ ($= \chi_{21}^0(2\mathbf{k}_0)$), corresponding to the inter-band process rather increases with decreasing temperature. The enhancement of the off-diagonal one comes from the fact that the electron-hole excitation across the ZGS can satisfy the nesting condition. Note that, at the zero temperature, the off-diagonal one does not diverge but has a finite value. This is ascribed to the ZGS with the vanishing of the density of state on the Fermi energy. Thus it is found that the $2\mathbf{k}_0$ density wave is mainly determined by the inter-band pairing.

Here we examine the effect of interaction on the density wave by calculating λ in eqs. (18) and (19). In addition to the direct effect of interaction by U and V , there is also the effect through $I_{\gamma\gamma'}$, which contains $\langle n_{\alpha} \rangle$ in ξ_{γ} . The variation of interactions are shown in Fig. 5, which denotes x -dependence of λ with $U = 0.4x$, $V_c = 0.17x$, $V_p = 0.05x$ ($0 \leq x \leq 1$). The set of interactions for $x = 1^{12}$ corresponds to the parameters, which are taken to explain the experimental result.² We note that, for $t_z = 0$, such a choice of interactions ($x = 1$) gives $T_C = 0$ due to $\lambda < 1$ while the further increase of $x (> 1)$ leads to a finite T_C with $\lambda = 1$. However such a T_C may be reduced to zero for $t_z = 0$ by the two-dimensional fluctuation. Within the present mean-field treatment, the increase of T_C is noticeable in the presence of the interlayer transfer t_z as shown later.

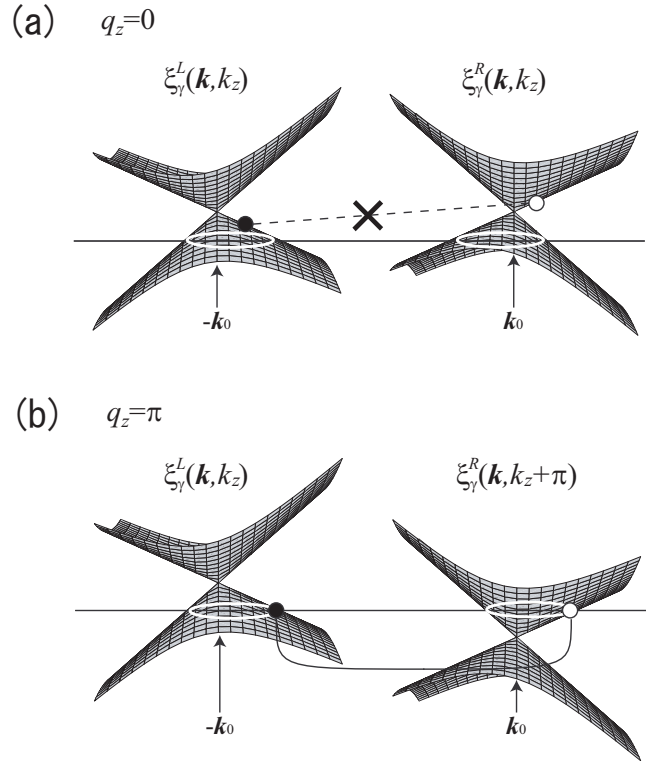


Fig. 6. Band dispersions $\xi_{\gamma}^{R,L}(\mathbf{k}, k_z)$ ($\gamma = 1, 2$) around $\mathbf{k} = \mathbf{k}_0$ and $-\mathbf{k}_0$ in the presence of t_z for (a): $q_z = 0$ and for (b): $q_z = \pi$, respectively. The Fermi surfaces are drawn by the white circle.

In Figs. 4 and 5, λ for the SDW and CDW states is calculated with the transfer energies at for $p = 16$ which is a reasonable pressure for the ZGS in the experiment.²⁴ The fact that $\lambda \propto x$ for small λ is understood as follows. The main effect of interaction comes from the coefficient of r.h.s. of eqs. (18) and (19) while the effect on $\langle n_{\alpha} \rangle$ is negligibly small. With increasing x in all the curve, the x -linear dependence is suppressed indicating that the enhancement of the charge disproportionation by interactions suppresses the density wave with $\mathbf{q} = 0$ and $2\mathbf{k}_0$. The reason for such a behavior partly comes from the suppression of the density of states close to the Fermi surface by the increase of the charge disproportionation. The density response with $\mathbf{q} = 2\mathbf{k}_0$ is larger than that with $\mathbf{q} = 0$. The increase for CDW as the function of x is due to the effect of V .

Although the $2\mathbf{k}_0$ -SDW state is the largest one among these four states, the magnitude of the interaction is not enough to obtain the finite T_C i.e. $\lambda = 1$ even for $x = 1$ in the present choice of parameters.

3.2 spin density wave in the presence of t_z

Based on the results of the previous subsection, we examine the SDW state, which leads to the finite T_C in the presence of t_z .

We note that T_C takes a maximum at $q_z = \pi$, i.e., the SDW with the interlayer variation being out of phase. This fact has been found in the quasi-one-dimensional density wave system, which consists of an array of chains coupled with the interchain electron hopping.³⁰ The typical q_z dependence of the present case appears in the main

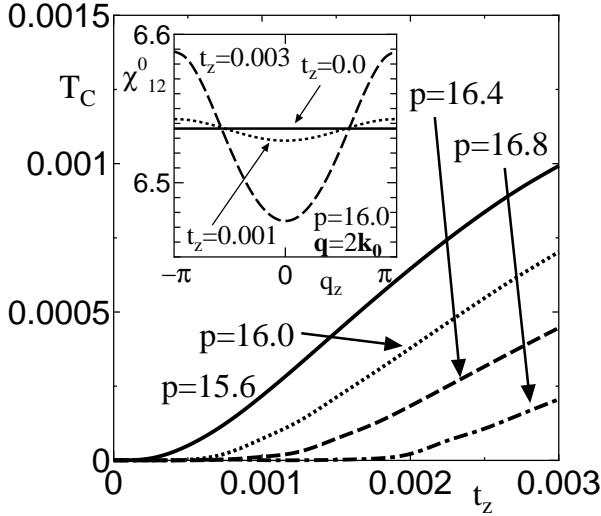


Fig. 7. t_z -dependences of T_C for $2\mathbf{k}_0$ -SDW state with $q_z = \pi$ for several pressures of $p = 15.6$ (solid line), 16.0 (dotted line), 16.4 (dashed line) and 16.8 (dot dashed line), where Coulomb interactions are chosen as $U = 0.4, V_c = 0.17, V_p = 0.05$. The inset figure is q_z -dependences of the inter-band susceptibility $\chi_{12}^0(2\mathbf{k}_0, q_z)$ given as eq. (22) for $t_z = 0.0$ (solid line), 0.001 (dotted line) and 0.003 (dashed line) at $p = 16$, where the temperature is set as $T = 0.001$.

contribution of the inter-band susceptibility $\chi_{12}^0(2\mathbf{k}_0, q_z)$. The inset of Fig. 7 displays $\chi_{12}^0(2\mathbf{k}_0, q_z)$, which takes a maximum at $q_z = \pi$ and a minimum at $q_z = 0$. The q_z dependence of the susceptibility is essentially given by $\chi_{12}^0(2\mathbf{k}_0, q_z) \propto \cos q_z$ due to the dispersion with $2t_z \cos k_z$ in eq. (9). Here, we note a fact that $\chi_{12}^0(2\mathbf{k}_0, q_z)$ takes a maximum at $q_z = \pm\pi$. In Fig. 6, a typical example of the band dispersion around the two contact points $\pm\mathbf{k}_0$ is shown, where ξ_γ^R and ξ_γ^L denote $\xi_\gamma(\mathbf{k}, k_z)$ ($\gamma = 1, 2$) for $\mathbf{k} \simeq \mathbf{k}_0$ and $\mathbf{k} \simeq -\mathbf{k}_0$, respectively. For $q_z = 0$, as shown in Fig. 6 (a), there is no contribution from the state with the wave number inside the circle of the Fermi surface, since electrons having ξ_γ^L and ξ_γ^R are both occupied or vacant, i.e. the inter-band process is absent. For $q_z = \pi$, on the other hand, the nesting condition is satisfied as shown in Fig. 6 (b), for the valence band of ξ_γ^L and the electron band of ξ_γ^R . As for the state outside of the circle of the Fermi surface, it is also found that the contribution of Fig. 6 (b) is larger than that of Fig. 6 (a). Thus, the inter-band process is enhanced by the appearance of two Fermi surfaces given by $\xi_{1(2)}^L$ with k_z and $\xi_{2(1)}^R$ with $k_z + \pi$, and the SDW is optimized at $q_z = \pi$.

In Fig. 7 the t_z dependence of T_C of the $2\mathbf{k}_0$ -SDW state is shown with some choices of pressures for $U = 0.4, V_c = 0.17, V_p = 0.05$. With increasing t_z , T_C increases noticeably while T_C for $t_z = 0$ is negligibly small. The increase of T_C for $q_z = \pi$ by t_z is ascribed to the grow of the Fermi surface of both valence and conduction bands, as drawn in Fig. 8, where the nesting condition is partly kept but is partly violated by t_z (e.g., there are two choices of pairings in Fig. 6 (b)). Note that $q_z = \pi$ is the relative momentum between ξ_γ^R and ξ_γ^L and then does not depend on the sign of t_z . The suppression of the SDW for $q_z = 0$ comes from a fact that the region of the Fermi

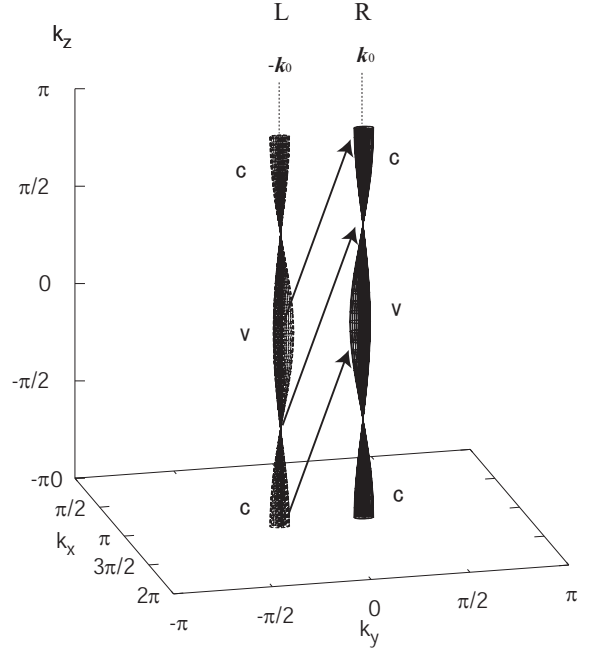


Fig. 8. Fermi surface in the three-dimensional momentum space, (k_x, k_y, k_z) , with k_z being the momentum along the interplane where $U = 0.4, V_c = 0.17, V_p = 0.05, p = 16$ and $t_z = 0.002$. The left one (L) and the right one (L) denote the Fermi surfaces around $-\mathbf{k}_0 = (-0.970\pi, -0.216\pi)$ and \mathbf{k}_0 , respectively, (for convenience, $-\mathbf{k}_0$ is replaced by that of the extended zone). The Fermi surface is given by the valence band (v) or by the conduction band (c), respectively, where the arrow denotes the nesting vector.

surface participating in the nesting condition is always reduced by t_z in spite of the emergence the Fermi surface. With increasing pressure, T_C is reduced rapidly due to the property of p -dependence of transfer energies, which increase the dip of the density of states around the Fermi energy under hydrostatic pressures, or the increase of the Fermi velocity under pressures.

4. Summary and Discussion

In summary, we have examined the role of interplane transfer energy on the SDW state in the ZGS of the α -(BEDT-TTF) $_2$ I $_3$ salt under the hydrostatic pressure. First, we estimated the pressure dependence of transfer energy. The ZGS appears at pressures higher than those of uniaxial strain along the stacking axis. Our result is qualitatively consistent with the experiment. Next, we studied the SDW in the presence of t_z and showed the increase of T_C with increasing t_z . Since the SDW originates from the electron-hole excitons between two Dirac cones with $\pm\mathbf{k}_0$, the nesting condition is reduced due to the Fermi point for the two-dimensional case of $t_z = 0$. Thus the appearance of the Fermi surface by t_z gives rise to the SDW.

Here we mention about the location of $\mathbf{q} = \mathbf{q}_{max}$, which gives the maximum value of T_C . Within the numerical accuracy of the present calculation, \mathbf{q}_{max} coincides with $2\mathbf{k}_0$ even for $t_z \neq 0$ although the deviation is generally expected. Actually \mathbf{q}_{max} becomes slightly different from $2\mathbf{k}_0$ for the case of the Zeeman energy, $-H_0 \sum_{i\alpha\sigma} \text{sgn}(\sigma) a_{i\alpha\sigma}^\dagger a_{i\alpha\sigma}$, instead of t_z ($\mu_B = 1$), where

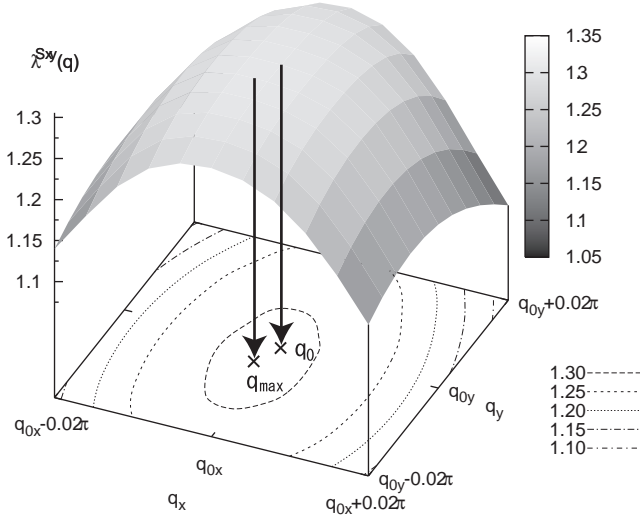


Fig. 9. \mathbf{q} -dependence of $\lambda^{S_{x,y}}$ in the presence of the Zeeman energy. Parameters are set as $U = 0.4, V_c = 0.17, V_p = 0.05, p = 16, H_0 = 0.003$ and $T = 0.001$, where $\mathbf{q}_0 = 2\mathbf{k}_0 = (-0.060\pi, 0.432\pi)$ and $\mathbf{q}_{max} = (-0.058\pi, 0.428\pi)$, respectively.

$\text{sgn}(\sigma) = 1(-1)$ for $\sigma = \uparrow(\downarrow)$. In the presence of H_0 , $\lambda^{S_{x,y}}$ increases but λ^{S_z} decreases. Note that the effect of H_0 on T_C of $S_{x,y}$ is nearly the same but is slightly large compared with t_z . Figure 9 shows an example of the contour plot of λ of $S_{x,y}$ on the plane of $\mathbf{q} = (q_x, q_y)$ close to $\mathbf{q} = 2\mathbf{k}_0 = (-0.060\pi, 0.432\pi)$, where the parameters are chosen as $U = 0.4, V_c = 0.17, V_p = 0.05$ with $p = 16$ and $H_0 = 0.003$. The location of the maximum is shown by the cross. Although the valence and conduction bands coincide at $\pm\mathbf{k}_0$, $\mathbf{q}_{max} = (-0.058\pi, 0.428\pi)$ is slightly different from $2\mathbf{k}_0$. Since the Dirac cone is anisotropic, the center of the Fermi surface with an ellipse is not located on \mathbf{k}_0 . Thus we can see the optimum wave number is near $\mathbf{q} = 2\mathbf{k}_0$ but is not exactly the same. On the other hand, \mathbf{q}_{max} for $t_z \neq 0$ is less effected since $t_z \cos k_z$ gives contribution corresponding to both $\pm H_0$.

We discuss the estimation of transfer energies and ZGS under the hydrostatic pressure. As shown in the previous section, the ZGS state under the hydrostatic pressure emerges at higher pressure compared with ZGS under uniaxial pressure p_a . This result is consistent with the experiment, since the temperature-independent behavior indicating the ZGS is observed at $p_a = 10$ (uniaxial pressure) and at $p = 20$ (hydrostatic pressure). However our result for ZGS state is still under smaller pressure. At high pressures with $p > 10$,²⁹ it is expected that the distortion is suppressed due to the deviation from the Hooke's law. Thus the increase of t_A by the pressure could be suppressed for that region and the ZGS is realized under higher pressure than our estimated one.

Finally, we note on the interlayer hopping. For simplicity, t_z is taken for the hopping, in which the electron moves into a site with the same index $\alpha (= 1, \dots, 4)$ of the adjacent layer, and then the position of the contact point is independent of k_z (see eq. (9)). However the hopping into other sites, which may reduce the nesting condition, is expected from the k_z dependence of the contact point as obtained by the first principle calcu-

lation.⁵ For the moment, there is no data of extended Hückel method for interlayer hoppings, and the role of the three-dimensionality remains as a future problem to clarify the properties of ZGS in α -(BEDT-TTF)₂I₃ salt.

Acknowledgements

We are grateful to N. Tajima, R. Kondo and H. Fukuyama for useful discussions. The authors also thank M. Tokumoto for informing us the reference concerning the hydrostatic pressure effect.²⁹ S. K. acknowledges the financial support of Research Fellowship for Young Scientists from Japan Society for the Promotion of Science (JSPS). This work also financially supported by a Grant-in-Aid for Scientific Research on Priority Areas of Molecular Conductors (No. 15073103) from the Ministry of Education, Culture, Sports, Science and Technology, Japan.

Appendix: Estimation of r_1 and r_2

We calculate quantities r_1 and r_2 from the data of the lattice parameters under the uniaxial strain²⁸ and hydrostatic pressure.²⁹ The variation of the lattice constants, which are defined as $u_a = (a(p_a, p_b) - a_0)/a_0$ for a -axis and $u_b = (b(p_a, p_b) - b_0)/b_0$ for b -axis, is written as

$$\begin{pmatrix} u_a \\ u_b \end{pmatrix} = - \begin{pmatrix} s_1 & s_2 \\ s_3 & s_4 \end{pmatrix} \begin{pmatrix} p_a \\ p_b \end{pmatrix}, \quad (\text{A}\cdot 1)$$

where $a_0 = a(0, 0)$ and $b_0 = b(0, 0)$. From eqs. (4) and (A-1), parameters r_1, r_2, s_1, s_2, s_3 and s_4 are related with the lattice distortion per unit pressure, E_j , ($j = 1, \dots, 6$). Actually we obtain

$$s_1 + s_2 = E_1, \quad s_3 + s_4 = E_2, \quad (\text{A}\cdot 2)$$

$$s_1 + s_2 r_1 = E_3, \quad s_3 + s_4 r_1 = E_4, \quad (\text{A}\cdot 3)$$

$$s_1 r_2 + s_2 = E_5, \quad s_3 r_2 + s_4 = E_6, \quad (\text{A}\cdot 4)$$

where eqs. (A-2), (A-3) and (A-4) correspond to the hydrostatic pressure, a -axis strain and b -axis strain, respectively. From the experimental results of the lattice distortion,^{28,29} E_i ($i = 1, \dots, 6$) are given as $E_1 = 0.00265 \text{ kbar}^{-1}$, $E_2 = 0.00247 \text{ kbar}^{-1}$, $E_3 = 0.00326 \text{ kbar}^{-1}$, $E_4 = 0.0 \text{ kbar}^{-1}$, $E_5 = 0.0 \text{ kbar}^{-1}$ and $E_6 = 0.00340 \text{ kbar}^{-1}$. By solving eqs. (A-2), (A-3) and (A-4), we obtain $s_1 = 0.00357 \text{ kbar}^{-1}$, $s_2 = -0.000917 \text{ kbar}^{-1}$, $s_3 = -0.00124 \text{ kbar}^{-1}$, $s_4 = 0.00371 \text{ kbar}^{-1}$, $r_1 = 0.335$ and $r_2 = 0.257$.

We note that quantities r_1, \dots, s_4 can be expressed in terms of Young's modulus, Y_a and Y_b , and Poisson's ratio, ν_{ab} and ν_{ba} , which are defined as

$$Y_a = \left(\frac{p_a}{u_a} \right)_{p_b=0}, \quad Y_b = \left(\frac{p_b}{u_b} \right)_{p_a=0} \quad (\text{A}\cdot 5)$$

$$\nu_{ab} = - \left(\frac{u_a}{u_b} \right)_{p_a=0}, \quad \nu_{ba} = - \left(\frac{u_b}{u_a} \right)_{p_b=0}. \quad (\text{A}\cdot 6)$$

Since $s_1 = 1/Y_a$, $s_2 = -r_2/Y_a$, $s_3 = -r_1/Y_b$, $s_4 = 1/Y_b$, we obtain $r_1 = \nu_{ba} Y_b / Y_a$ and $r_2 = \nu_{ab} Y_a / Y_b$.

- 1) H. Seo, C. Hotta and H. Fukuyama: *Chem. Rev.* **104** (2004) 5005.
- 2) N. Tajima, A. Ebina-Tajima, M. Tamura, Y. Nishio and K. Kajita: *J. Phys. Soc. Jpn.* **71** (2002) 1832.
- 3) S. Katayama, A. Kobayashi and Y. Suzumura: *J. Phys. Soc. Jpn.* **75** (2006) 054705.
- 4) S. Ishibashi, T. Tamura, M. Kohyama and K. Terakura: *J. Phys. Soc. Jpn.* **75** (2006) 015005.
- 5) H. Kino, T. Miyazaki: *J. Phys. Soc. Jpn.* **75** (2006) 034704.
- 6) N. Tajima, M. Tamura, Y. Nishio, K. Kajita and Y. Iye: *J. Phys. Soc. Jpn.* **69** (2000) 543.
- 7) S. Katayama, A. Kobayashi and Y. Suzumura: *J. Phys. Soc. Jpn.* **75** (2006) 023708.
- 8) Y. Takano, K. Hiraki, H. M. Yamamoto, T. Nakamura and T. Takahashi: *Synth. Met.* **120** (2001) 1081.
- 9) H. Kino and H. Fukuyama: *J. Phys. Soc. Jpn.* **64** (1995) 4523.
- 10) H. Seo: *J. Phys. Soc. Jpn.* **69** (2000) 805.
- 11) A. Kobayashi, S. Katayama, K. Noguchi and Y. Suzumura: *J. Phys. Soc. Jpn.* **73** (2004) 3135.
- 12) A. Kobayashi, S. Katayama and Y. Suzumura: *J. Phys. Soc. Jpn.* **74** (2005) 2897.
- 13) J. W. McClure, *Phys. Rev.* **104** (1956) 666.
- 14) J. C. Slonczewski and P. R. Weiss: *Phys. Rev.* **109** (1958) 272.
- 15) P. A. Wolff: *J. Phys. Chem. Solids* **25** (1964) 1057.
- 16) H. Fukuyama and R. Kubo: *J. Phys. Soc. Jpn.* **28** (1970) 570.
- 17) H. Kohno, H. Yoshioka and H. Fukuyama: *J. Phys. Soc. Jpn.* **61** (1992) 3462.
- 18) T. Ando: *J. Phys. Soc. Jpn.* **74** (2005) 777.
- 19) T. Ando, T. Nakanishi, and R. Saito: *J. Phys. Soc. Jpn.* **67** (1998) 2857.
- 20) K. S. Novoselov, A. K. Geim, S. V. Morozov, D. Jiang, M. I. Katsnelson, I. V. Grigorieva, S. V. Dubonos and A. A. Firsov: *Nature* **438** (2005) 197.
- 21) Y. Zhang, Y. W. Tan, H. L. Stormer and P. Kim: *Nature* **438** (2005) 201.
- 22) A. Kobayashi, S. Katayama, Y. Suzumura and H. Fukuyama: *J. Phys. Soc. Jpn.* **76** (2007) 034711.
- 23) J. M. Luttinger and W. Kohn: *Phys. Rev.* **97** (1955) 869.
- 24) N. Tajima, S. Sugawara, M. Tamura, Y. Nishio and K. Kajita: *J. Phys. Soc. Jpn.* **75** (2006) 051010.
- 25) E. V. Gorbar, V. P. Gusynin, V. A. Miransky and I. A. Shovkovy: *Phys. Rev. B* **66** (2002) 045108.
- 26) Y. Kopelevich, J. H. S. Torres, R. R. da Silva, F. Mrowka, H. Kempa and P. Esquinazi: *Phys. Rev. Lett.* **90** (2003) 156402.
- 27) Y. Kopelevich, J. C. Medina, R. R. da Silva and S. Moehlecke: *Phys. Rev. B* **73** (2006) 165128.
- 28) R. Kondo, S. Kagoshima and J. Harada: *Rev. Sci. Instrum.* **76** (2005) 093902.
- 29) I. Tamura, H. Kobayashi and A. Kobayashi: *J. Phys. Chem. Solids* **76** (2002) 1255.
- 30) Y. Suzumura and H. Fukuyama: *J. Low Temp. Phys.* **31** (1978) 273.